IAEA
International Atomic Energy Agency

20th IAEA Fusion Energy Conference
Vilamoura, Portugal, 1-6 November 2004

IAEA-CN-116/TH/P6-2

Convective Transport in Tokamaks

D. A. D'Ippolito, J. R. Myra and D. A. Russell
Lodestar Research Corporation, Boulder, Colorado, USA

S. I. Krasheninnikov, A. Yu. Pigarov, and G. Q. Yu
University of California, San Diego, La Jolla, California, USA

X. Q. Xu and W. M. Nevins
Lawrence Livermore National Laboratory, Livermore, California, USA

Convective Transport in Tokamaks

D. A. D'Ippolito,[1] J. R. Myra,[1] D. A. Russell,[1] S. I. Krasheninnikov,[2] A. Yu. Pigarov,[2] G. Q. Yu,[2] X. Q. Xu,[3] and W. M. Nevins,[3]

[1]Lodestar Research Corporation, Boulder, Colorado, USA
[2]University of California San Diego, La Jolla, California, USA
[3]Lawrence Livermore National Laboratory, Livermore, California, USA

e-mail contact of main author: dippolito@lodestar.com

Abstract. Scrape-off-layer (SOL) convection in fusion experiments appears to be a universal phenomenon that can "short-circuit" the divertor in some cases. The theory of "blob" transport provides a simple and robust physical paradigm for studying convective transport. This paper summarizes recent advances in the theory of blob transport and its comparison with 2D and 3D computer simulations. We also discuss the common physical basis relating radial transport of blobs, pellets, and ELMs and a new blob regime that may lead to a connection between blob transport and the density limit.

1. Introduction

Convection of coherent objects (blobs, ELMs and pellets) is a general and important phenomenon in fusion plasmas. Extensive experimental, theoretical, and computer simulation work has been devoted to the study of spatially- and temporally-intermittent convection in the SOL of toroidal and linear machines (see references in [1]-[2]). This rapid radial convection can "short-circuit" the divertor in fusion experiments, leading to increased interaction of the plasma with the first wall.

The theory of blob transport [1] provides a simple and robust physical paradigm for studying SOL convective transport. The nonlinear development of edge turbulence gives rise to objects with enhanced density, temperature, and vorticity which propagate as coherent structures. These turbulent objects look like filaments along the field line ($L_\perp << L_\parallel$) but resemble localized "blobs" $\perp$ **B**. These blobs are convected across the SOL due to the action of an outwards force **F** (e.g. curvature, neutral friction, or centrifugal; see Sec. 2). The blob model is a simplified representation of the turbulent structures, but it makes quantitative predictions about their radial motion based on the charge sources and sinks in the SOL.

The analytic sheath-connected blob model [1] shows reasonable agreement with 2D simulations [3-8] in which density blobs are initialized and their subsequent ballistic motion computed including non-ideal effects, background density, and the effect of secondary instabilities. Although born from turbulent processes, blobs of the size seen in experiments are stable on the transport timescale according to these simulations. Other 2D simulations have studied intermittent particle transport [9,10] and blob production [10] in the SOL due to interchange turbulence [11]. Recently, this work was extended by 3D computer simulations [12,13] of resistive ballooning and RX-mode turbulence (see Sec. 3). These simulations confirmed that blobs are produced by turbulence, but a generalization of the blob theory was required to explain the blob dynamics observed in the 3D simulations.

One of the key insights from this work is that the blob polarization potential Φ and velocity $\mathbf{v} = (c/B)\,\mathbf{b}\times\nabla\Phi$ are controlled by the voltage-current relation $J_\parallel(\Phi)$ associated with the flow of charge. This relation depends on the axial boundary condition (BC) imposed by the

physical parameters of the region where the blob terminates. Consideration of more general BCs (e.g. in X-point geometry or at finite plasma β) has extended the blob model to 3D and led to the discovery of several blob regimes which have different scalings with the strength of the force, the collisionality, and the blob size, and which correspond to the linear instability regimes that give rise to the blobs (see Sec. 4). Recent work shows a common physical basis relating blob, pellet, and ELM radial transport [see Sec. 2.3 and Ref. 14] and suggests a relation between blob transport and the density limit (see Sec. 5).

In the rest of this paper unless otherwise noted, we use dimensionless variables: $n/n_0 \rightarrow n$, $T_e/T_{e0} \rightarrow T_e$, $\Omega_i\, dt \rightarrow dt$, $\rho_s\nabla \rightarrow \nabla$, $v/c_s \rightarrow v$, $\mathbf{J}/(n_s e c_s) \rightarrow \mathbf{J}$, $e\Phi/T_{es} \rightarrow \Phi$, $\sigma/\sigma_0 \rightarrow \sigma$, where $\Omega_i = eB/m_i c$, $\rho_s = c_s/\Omega_i$, $c_s = (T_{e0}/m_i)^{1/2}$, $\sigma_0 = \omega_{pi}^2/(4\pi\Omega_i) = (nec/B)$, and n_0 and T_{e0} are reference values.

2. Blob Dynamics

2.1. Physical Mechanism of Blob Transport

When an outwards force **F** acts on a localized density enhancement ("blob"), the species dependent **F**×**B** drift causes a charge polarization of the blob. The induced electric field **E** in the **F**×**B** direction causes an **E**×**B** drift of the blob *outwards* in the direction of **F** [1]. Examples include the ∇B "force" due to toroidal curvature [1], the centrifugal force in linear experiments, and certain neutral frictional forces ("neutral wind") [15]. Thus, the blob mechanism is robust and almost universal in confined plasmas. [Structures with local density depletion ("holes") transport *inwards* by the same mechanism and may play a role in impurity transport.] Many of the familiar linear instability drives in the SOL are known to have nonlinear dynamics which support convective propagation of coherent structures. In addition to the curvature drive, the long wavelength, nonlinear limit of the ∇T-sheath and parallel-velocity-shear instabilities have also recently been explored [16].

The ingredients for blob (hole) transport are: (i) an outwards force **F**; (ii) a local density enhancement (or depletion); and (iii) sufficient resistance to charge flow to ensure that the blob polarization potential Φ and induced electric field **E** survive on the transport time scale. The charges can be dissipated by parallel current flow $J_{||}$ along **B** or mixed (recombined) by blob spin [6]. A schematic of the blob polarization physics is shown in Fig. 1.

Blob spin occurs for blobs (or ELMs) which are hotter than the surrounding plasma and are electrically connected to the sheaths at the end walls (requiring large conductivity $\sigma_{||}$). Their spin results from the internal electric field $E_r = -\nabla_r\Phi_B$, where $\Phi_B \approx 3T_e$ is the Bohm sheath potential and $T_e(r)$ is the centrally-peaked blob temperature profile. 2D computer simulations and analytic calculations in Ref. 6 show that the blob spin averages out the curvature-induced charge polarization when the spin is fast enough, viz. $\Omega\tau_{||}/a^2 >> 1$, where Ω is the angular velocity, $\tau_{||}$ is the parallel loss time, and *a* is the blob radius in units of ρ_s. When this condition is satisfied the blobs do not move radially and can develop an m = 2 rotational instability [7].

In what follows, we consider non-spinning blobs, take T_e = const. for simplicity, and focus the discussion on blobs in diverted tokamak geometry. The coordinates (x,y,z) denote the directions **F**, **–F**×**B,** and **B**, respectively, in the outer midplane of the tokamak.

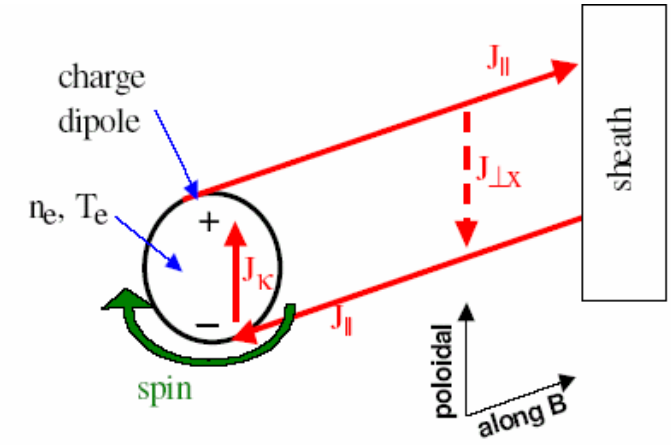

Fig. 1 Blob schematic showing the charge accumulation produced by the curvature-driven current and the two mechanisms for reducing the charge build-up: spin and parallel currents. The current path is closed by perpendicular currents in the plasma (e.g. near the X-points) or in the sheaths.

2.2. Blob Voltage-Current Relation and BCs

In the absence of spin, the blob dynamics are controlled by the parallel flow of charge which determines the blob voltage-current relation $J_{||}(\Phi)$. Consideration of the blob current path is a useful way to build up intuition regarding blob parameter regimes. The **F**×**B** drift provides essentially a fixed current source I to the blob "circuit"; the potential Φ and radial velocity $v_x = -\partial\Phi/\partial y$ at the outer midplane therefore increase in proportion to the total resistance $\Re$ of the blob current path ($\Phi = \Re I$). The resistance $\Re$ has contributions from the plasma resistances parallel ($\Re_{||} \propto \sigma_{||}^{-1}$) and perpendicular ($\Re_\perp$) to **B** and from the sheath resistance ($\Re_{sh}$), which are proportional to the plasma and sheath resistivities. The perpendicular current $\mathbf{J}_\perp$ can be large in the SOL of a diverted tokamak, especially near the X-points, closing the current loop and modifying Φ and v_x.

The quantities Φ, $J_\perp$ and $J_{||}$ can vary along the field lines in the divertor region (and detach from the plates) because of the increased resistivity of the cooler plasma near the divertor ($\Rightarrow$ larger $\Re_{||}$) and the enhanced $\mathbf{J}_\perp$ ($\Rightarrow$ smaller $\Re_\perp$) near the X-points. The latter effect occurs because the blob flux tube undergoes an elliptical distortion near the X-point, which enhances current flow across the thin part of the fan [14,17]. The original blob theory [1] assumed small plasma resistivity ($\Re_\perp, \Re_{||} << \Re_{sh}$) so that the blob velocity was governed by sheath resistivity and the blob had no variation along **B**. More recently, we have explored high-density and high-β regimes in which the blob structure is three-dimensional and its velocity is governed by other physics, as described below.

The blob dynamics is governed by the dimensionless vorticity equation

$$n\frac{d}{dt}\nabla_\perp^2\Phi = \nabla_{||} J_{||} - 2\kappa\frac{\partial n}{\partial y} \quad , \qquad (1)$$

where $d/dt = \partial/\partial t + \mathbf{v}\cdot\nabla$, $\mathbf{b}\cdot\nabla\mathbf{b} = -\kappa\mathbf{e}_x$ is the magnetic curvature ($\kappa = 1/R_c$) and $\mathbf{b} = \mathbf{B}/B$. The terms in Eq. (1) represent the divergence of the ion polarization current, the parallel current, and the curvature-drift current, respectively. This relation must be supplemented by Ohm's Law and an axial BC. Various analytic solutions of this system have been obtained to illustrate the parameter space of blobs.

The simplest case has $\Re_{||} << \Re_{sh} << \Re_\perp$ so that the current flow is dominated by the sheath resistivity and $\Phi(z)$ is approximately constant between the divertor plates at $z = \pm L_{||p}$. We

integrate Eq. (1) between the plates, and the $\nabla_{||}J_{||}$ term yields the boundary term $2J_{||}/L_{||p}$. This is evaluated using the sheath BC expanded for $\Phi << 1$, viz. $J_{||}(\pm L_{||p}) = \alpha_{sh}\Phi$, where $\alpha_{sh} = 1/L_{||p} \propto 1/\Re_{sh}$. Neglecting the first term in Eq. (1) and taking $\partial n/\partial y \sim n/a$, we balance the sheath and curvature terms to obtain the original 2D sheath-connected blob solution [1]: $\Phi = q/a$ and $v_x \equiv v_{x0} = (q/a^2)$, where $q \equiv 2\kappa/\alpha_{sh} \sim L_{||p}/R_c$. This solution is easily generalized to the case where the parallel resistivity is important ($\Re_{||}/\Re_{sh} \sim 1$):

$$v_x = v_{x0}\,(1+\Lambda) \quad , \tag{2}$$

where the *collisionality parameter* $\Lambda \equiv (ne^2c_sL_{||p}/T_e\sigma_{||}) = (m_e/m_i)^{1/2}\,(L_{||p}/\lambda_{ei})$ is a measure of $\Re_{||}/\Re_{sh}$, the dimensional $\sigma_{||} = (2ne^2/m_e\nu_e)$ and $\lambda_{ei} = v_{the}/\nu_e$ is the electron mean free path.

Other solutions (valid at higher densities where $\Re_{||} >> \Re_{\perp}$) have been obtained by integrating Eq. (1) between the X-points (at $z = \pm L_{||x}$) and applying a BC on $J_{||}(\pm L_{||x})$, assuming that $\Re_{\perp}$ is small and $\Re_{||}$ large in the divertor. We match $J_{||}$ at the X-points to a solution of Eq. (1) in the divertor region which retains the physics of $\mathbf{J}_{\perp}$ and the sheath BC, but neglects the curvature source term. For example, a simple result is obtained in the linearized electrostatic approximation ($J_{\perp} = -i\,k_{\perp}\sigma_{\perp}\Phi$, $J_{||} = -\sigma_{||}\nabla_{||}\Phi$) taking the eikonal limit ($-i\nabla_{\perp} \rightarrow k_{\perp} \sim 1/a$) and assuming that $\mathrm{Im}[k_{||}(z)] \equiv p(z) = k_{\perp}(\sigma_{\perp}/\sigma_{||})^{1/2} =$ constant. The relation $\nabla\cdot\mathbf{J} = 0$ implies the following BC [18] for the parallel current at the X-points:

$$J_{||}\left(\pm L_{||x}\right) = \pm k_{\perp}\left(\sigma_{\perp}\sigma_{||}\right)^{1/2}\Phi\left(\pm L_{||x}\right) \quad , \tag{3}$$

which again has the form $J_{||} = \alpha_x\,\Phi$. When the disconnection condition $p(L_{||p} - L_{||x}) >> 1$ is satisfied, the blob is fully disconnected from the sheaths for $z > L_{||x}$, and one obtains an exponentially decaying solution $\Phi(z) \propto \exp(-pz)$. The radial velocity is then given by

$$v_x = v_{x0}\left(\Lambda/D\right) \quad , \tag{4}$$

where $D \equiv pL_{||x} \propto (\sigma_{\perp}/\sigma_{||})^{1/2}$ and $\Lambda/D \propto (\sigma_{\perp}\sigma_{||})^{-1/2}$. This solution is valid for arbitrary $\sigma_{\perp}$. The case where $\sigma_{\perp}$ is due to electron-ion collisions was considered in Refs. [14,18] and a heuristic application of this solution to the case of the nonlinear ion polarization current ($\sigma_{\perp} \sim \Phi/a^2$) was used in Ref [13]. Taking into account the flux tube ellipticity factor $E >> 1$ ($p \rightarrow pE$) makes it relatively easy to satisfy the disconnection condition near the separatrix, $pE(L_{||p} - L_{||x}) >> 1$.

In the high-collisionality (large ν_e) limit, $\Lambda/D >> 1$, Eq. (4) predicts that the blob transport far exceeds the value predicted by the simple 2D sheath-connected model. This limit requires (i) $\Re_{\perp} << \Re_{||}$ for the blob current loop to close across the X-points rather than by parallel currents, and (ii) $\Re_{sh} << (\Re_{\perp}\Re_{||})^{1/2}$ for the disconnected blob to move faster. Both of these conditions can be met by local cooling of the divertor region. The disconnected blob regime is needed to understand the 3D turbulence simulations (Sec. 3) and it may be relevant to the convective density limit (Sec. 5).

2.3. Alfvén Wave BC and relation to ELMs and Pellets

For simplicity, we restrict the discussion of finite-β effects in this section to the ideal MHD limit. The electrostatic (ES) limit discussed in Sec. 2.2 applies when $\partial_t \sim \mathbf{v}_{\perp}\cdot\nabla >> v_a\nabla_{||}$. In the finite-β limit where Alfvén waves propagate $\left(\partial_t \sim v_a\nabla_{||}\right)$, electromagnetic (EM) effects

can determine the blob dynamics. Here β is the ratio of the thermal pressure inside the blob to magnetic pressure. We consider blobs that are localized (in z) near the midplane between two finite-β regions, where outgoing Alfvén waves provide the axial BC that completes the blob circuit. Finite-β blobs may be produced by ELM crashes.

The treatment of this problem [14] is similar to the one used to study the evolution of plasma clouds (e.g. due to pellet injection) [19]. In the Alfvén wave region, $J_{||}$ is determined by combining Ampere's Law $J_{||} = \left(\nabla_\perp{}^2 A_{||}\right)/\beta$ (in the Coulomb gauge) and Ohm's Law ($E_{||} = 0$) in the form $\partial_t A_{||} = -\nabla_{||}\Phi$, so that $J_{||} = \pm\beta^{-1/2}\ \nabla_\perp{}^2\Phi$, where the sign is chosen to give outgoing waves. This Alfvén wave BC on $J_{||}$ is analogous to Eq. (3) in the high-collisionality case. Integrating Eq. (1) along **B** and matching $J_{||}$ at the entrance to the Alfvén region, the following dynamical equation is obtained

$$\frac{d}{dt}\nabla_\perp^2\Phi = \left(2n_a/nL_{||}\beta^{1/2}\right)\nabla_\perp^2\Phi - \frac{2\kappa}{n}\frac{\partial n}{\partial y} \quad , \tag{5}$$

where n and n_a are the densities in the midplane and Alfvén wave regions, respectively. Here, the dimensionless variables defined in Sec. 1 are employed with $\beta = c_s{}^2/v_a{}^2$ and $v_a{}^2 = B^2/(4\pi n m_i)$. This solution is self-consistent when the field lines bend sufficiently in the radial direction that the blobs terminate in the hot plasma inside the last closed flux surface (LCFS). The latter situation can occur when β is large enough [14], viz. $\beta > R\Delta_w/L_{||a}{}^2$, where Δ_w is the distance from the LCFS to the wall and $L_{||a}$ the scale length in the Alfvén region. An order of magnitude estimate obtained by balancing the last two terms in Eq. (5) gives

$$v_x \sim \Phi/a \sim \left(n/n_a\right) q_a\, \beta^{1/2} \quad , \tag{6}$$

where $q_a = L_{||a}/R_c$. A numerical solution of Eq. (5) confirms the prediction that v_x is independent of blob size *a* (Eq. (6)) and shows that the blob maintains its stability while moving large distances. Interestingly, Eq. (5) also describes the evolution of ionospheric plasmas where the dissipative mechanism is due to plasma-neutral collisions [20].

Finally, when $\partial_t << v_a\nabla_{||}$, a finite-β solution has been obtained [21] in which EM effects disconnect and accelerate the blobs and lead to a density limit.

3. 3D BOUT code simulation of blobs

Recently, 3D simulations were carried out to study the production and dynamics of blobs in a 3D diverted tokamak [13]. The BOUT turbulence code was used [12], which employs the Braginskii fluid equations and 3D tokamak geometry with magnetic separatrix and X-points. A new set of blob diagnostic tools [13], based on the GKV visualization package [22], were developed and used to analyze the blob dynamics in the simulation.

The simulation was fueled by neutral particle injection concentrated about the X-point in a diverted, DIII-D deuterium plasma [13]. The plasma density was observed to increase with time and eventually saturate in a state of strong turbulence characterized by *order unity fluctuations*. The blob emission rate increased dramatically after the average density saturated at $\langle n\rangle = 1.5 \times 10^{13}$ / cm^3 (at the outboard midplane separatrix), where $\langle T_e\rangle = 28$ eV and $B_0 = 2.3$ T. Figure 2 shows contours of density superimposed on a plot of the charge density

(vorticity). Each density peak coincides with a dipole charge pattern consistent with the curvature-driven polarization picture of the blob model (e.g. see the circled blob).

A blob database was extracted from this simulation. Blob trajectories were identified and the radial velocities were computed and compared with the theoretical models described in Sec. 2.2. The velocity was in the range v_x = 1-6 km/s, where c_s = 20-30 km/s in the SOL. This is much larger than predicted by the 2D sheath-connected blob model. Moreover, the blob's T_e pattern was a dipole, rather than the monopole expected from the 2D theory. Estimates indicate that the simulation is in the low-β ES regime. These puzzles led us to develop the 3D disconnected blob theory (see Eq. [4]), which agrees with the simulation when we take into account the Braginskii thermal physics terms ($\Rightarrow T_e$ dipole) and assume that the blob current loop is closed at the X-points by the ion polarization current, $\mathbf{J}_{\perp pol} \equiv -\sigma_{\perp pol} \nabla_\perp \phi \sim \sigma_{\perp pol}\, \phi/a$, where $\sigma_{\perp pol} = (c^2\Omega_i/4\pi v_A^2)\,(e\phi/T_e)\,(\rho_s/a)^2 \propto \phi/a^2$. More details are given in Ref. [13].

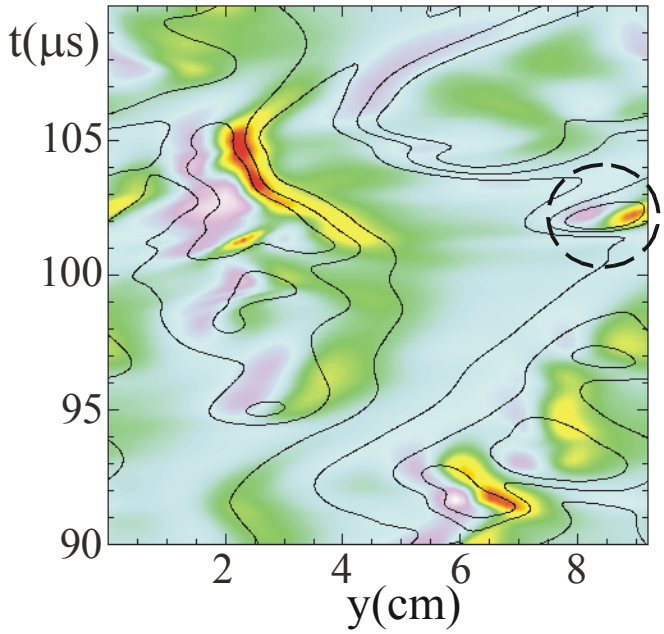

Fig. 2 Ion density contour lines superimposed on an intensity plot of charge density (red: positive, blue: negative). These contours are shown in the y-t plane at a radial location (x = 3 cm) outside of the turbulent blob creation zone.

In summary, the simulations and model reported in [13] show that: (1) blobs arise in the nonlinear stages of ballooning and RX-mode turbulence and propagate outwards; (2) the curvature drift creates the charge dipole and corresponding **E**×**B** drift v_{Ex}, as in the 2D theory, but v_{Ex} is larger in the 3D theory because the blob voltage-current relation now gives $e\phi/T_e \sim 1$; (3) $J_{||}$ disconnects from the sheaths because of the small $\sigma_{||}$ (due to ionization-induced cooling) and large $\sigma_\perp$ (due to the elliptical flux tube distortion) in the X-point region; (4) the X-point "short-circuiting" of $J_{||}$ establishes a temperature dipole in phase with the charge and vorticity dipoles; (5) blob disconnection by ion polarization drifts is related to the physics of the resistive X-point (RX) mode turbulence [23] which describes the linear phase of the simulations [24].

4. Scaling of blob transport

Several blob regimes differing in their physical assumptions and BCs were discussed in Secs. 2 and 3. Here, we summarize the scaling of the radial blob velocity in each regime restoring the dimensional factors. In ES blob theory, the 2D sheath-connected regime [1], extended to include both sheath and plasma resistivity, has the scaling

$$v_x = c_s \left(L_{||p}/R_c\right)(1+\Lambda)\left(\rho_s/a\right)^2 \quad . \qquad (7)$$

In the high-collisionality divertor limit, fully-disconnected 3D blobs with $\mathbf{J}_\perp$ at the X-points provided by (i) electron-ion collisions [14] and (ii) ion polarization currents (Sec. 3 and [13]), have the scalings:

$$\begin{aligned} &\text{(i)} \quad v_x \approx c_s \ (L_{\|x}/R_c)(\rho_s/a) \quad , \\ &\text{(ii)} \quad v_x \approx c_s \ (L_{\|x}/R_c)^{2/3}(\rho_s/a)^{1/3} \ (\nu_e/2\Omega_e)^{1/3} \quad . \end{aligned} \tag{8}$$

Finally, the finite-β EM blob / ELM / pellet discussed in Sec. 2.3 has the scaling:

$$v_x = c_s \ \beta^{1/2}(L_{\|a}/R_c)(n_a/n) \ . \tag{9}$$

The scaling of $v_x(a)$ differs in each of these blob regimes, and each regime corresponds to a linear instability regime [25]: e.g. Eq. (7) ⇔ sheath-interchange instability, Eq. (8) (ii) ⇔ ES resistive X-point (RX) modes [23], and Eq. (9) ⇔ EM RX-modes.

5. Blob-induced density limit

A convective density limit has been observed on C-Mod [26,27]: as n and ν_e increase, a region of enhanced cross-field transport (flattened n and T_e profiles) extends inwards from the wall towards the separatrix. As $\bar{n}/n_G \to 1$ (n_G is the Greenwald density limit), this region crosses the separatrix, and the perpendicular convective energy flow $Q_\perp$ exceeds the parallel conductive energy flow $Q_\|$ near the separatrix (see Fig. 26 in Ref. [27]). The resulting cooling leads to the experimentally-observed density limit. (Here, $Q_\perp = q_\perp A_\perp$ and $Q_\| = (\nabla_\| q_\|)A_\|$ with heat fluxes $q_\perp = T_e\, n v_x$ and $q_\| = -\kappa_{\|e}\nabla_\| T_e \propto -T_e^{5/2}\nabla_\| T_e$.)

The disconnected blob model provides a plausible mechanism for the strong cross-field transport observed near the density limit on C-Mod and seen in simulations [28,29]. In Sec. 2.2 we showed that the blob velocity v_x increases with the collisionality parameter $\Lambda \propto \nu_e$ [Eqs. (2) and (4)], so that enhanced particle and heat transport is expected at higher ν_e. The underlying cause is that X-point cooling increases $\Re_\| \propto \sigma_\|^{-1}$ and thus the total resistance of the blob current path, leading to an increased polarization potential Φ, as observed in the high-density turbulence simulations described in Sec. 3. A blob-induced density limit receives further support from the gas-puff-imaging (GPI) diagnostic results on C-Mod. The GPI data shows that at high density $(\bar{n}/n_G \geq 0.75)$ blobs are generated inside the separatrix [30]. The measured edge n and T_e profiles on the same shots show T_e dropping inside the separatrix and the intermittency increasing there.

Work is in progress [31] to model this density limit for various blob scenarios with and without radiation. When $Q_\perp > Q_\|$, the temperature drops in the X-point region; the increased collisionality leads to further blob detachment and a subsequent increase in the blob v_x and $q_\perp$. This process may lead to loss of thermal equilibrium in the midplane region (with resulting current channel collapse and MHD disruption) or to thermal instability, e.g. X-point MARFEs (as reported in [29]). Note that there is a synergy between blob transport and MARFE formation because the blob convection circumvents the (stabilizing) parallel heat flow to the X-point.

6. Summary

Some recent developments in blob theory have been described. A number of new 3D blob regimes having different axial BCs have been explored, including a high-density collisional regime relevant to the density limit, and a finite-β regime relevant to ELMs and similar in spirit to plasma cloud (pellet) solutions. These regimes have a direct correspondence with the linear instability physics that produces the blobs. The blob voltage-current relation is a useful framework for understanding the scaling of the radial blob velocity. 3D BOUT turbulence simulations confirm that blobs are produced by 3D tokamak turbulence and that the blob dynamics changes at high collisionality (becoming disconnected from the sheaths). The increased blob velocity at high-ν_e may be related to the C-Mod convective density limit.

References

[1] Krasheninnikov, S.I., Phys. Letters A, **283** (2001) 368; D'Ippolito, D.A., Myra, J.R., and Krasheninnikov, S.I, Phys. Plasmas **9** (2002) 222.
[2] D'Ippolito, D. A., Myra, J.R., Krasheninnikov, S.I, et al., Contr. Plasma Phys. **44** (2004).
[3] Bian, N., Benkadda, S., Paulsen, J.-V., and Garcia O.E., Phys. Plasmas **10** (2003) 671.
[4] D'Ippolito, D.A., and Myra, J.R., Phys. Plasmas **10** (2003) 4029.
[5] Yu, G. Q., and Krasheninnikov, S.I., Phys. Plasmas **10** (2003) 4413.
[6] Myra, J.R., D'Ippolito, D.A., et al., Phys. Plasmas **11** (2004) 4267.
[7] D'Ippolito, D.A., Myra, J.R., Russell, D.A. et al., Phys. Plasmas **11** 4603 (2004).
[8] Bisai, N., et al., Phys. Plasmas **11** (2004) 4018.
[9] Sarazin, Y., and Ghendrih, Ph., Phys. Plasmas **5** (1998) 4214.
[10] Garcia, O.E., Naulin, V., Nielsen, A.H., et al., Phys. Rev. Lett. **92** (1994) 165003-1.
[11] Nedospasov, A.V., et al., Nucl. Fusion **25** (1985) 21; Endler, M., et al., Nucl. Fusion **35** (1995) 1307.
[12] Xu, X.Q., et al., Phys. Plasmas **10** (2003) 1773; Xu, X.Q., et al., Bull. APS **48** (2003) KP1-20.
[13] Russell, D.A., D'Ippolito, D.A., Myra, J.R., Nevins, W.M., and Xu, X.Q., Lodestar Report #LRC-04-99, June, 2004, submitted to Phys. Rev. Lett.
[14] Krasheninnikov, S.I., Ryutov, D.D., and Yu, G.Q., *International Toki Conference 2003*, to be published in Journal of Plasma and Fusion Research (2004).
[15] Krasheninnikov, S.I., and Smolyakov, A.I., Phys. Plasmas **10** (2003) 3020.
[16] Krasheninnikov, S.I., et al., *31st EPS Conference on Plasma Phys*., London, P-1.103 (2004).
[17] Farina, D., Pozzoli, R., Ryutov, D., Nucl. Fusion **33** (1993) 1315.
[18] Ryutov, D.D., and Cohen, R.H., Contrib. Plasma Phys. **44** (2004) 168.
[19] Rozhansky, V., et al., Plasma Phys. Control. Fusion **37** (1995) 399; Parks, P.B., et al., Phys. Plasmas **7** (2000) 1968.
[20] Sudan, R.N., et al., Phys. Reports **283** (1997) 95.
[21] Myra, J.R., et al., *29th EPS Conference on Plasma Phys.*, Montreux, 2002, O-3.23.
[22] Nevins, W.M., GKV manual in preparation (2004).
[23] Myra, J.R., D'Ippolito, D.A., Xu, X.Q., and Cohen, R.H. Contrib. Plasma Phys. **40** (2000) 352.
[24] X. Q. Xu et al., New Journal Phys. **4**, 53.1 (2002).
[25] Myra, J.R., D'Ippolito, D.A., and Russell, D.A., Bull. APS **49** (2004), paper CP1.065.
[26] LaBombard, B., Boivin, R.L., Greenwald, M., et al., Phys. Plasmas **8** (2001) 2107.
[27] Greenwald, M., Plasma Phys. Contr. Fusion **44** (2002) R27.
[28] Xu, X. Q., Nevins, W.M., Rognlien, T.D., et al., Phys. Plasmas **10** (2003) 1773.
[29] Xu, X. Q., Cohen, R.H., Nevins, W.M., et al., this meeting.
[30] Terry, J.L., Zweben, S.J., et al., Phys. Plasmas **10**, 1739 (2003); Terry, J.L., et al., this meeting.
[31] D'Ippolito, D.A., Myra, J.R., and Russell, D.A., Bull. APS **49** (2004), paper PP1.062.